

## ソリトン理論の最近の話題—超離散の応用と交通流—

Recent development in Soliton theory

– Ultradiscrete method and its applications –

龍谷大学 理工学部 西成 活裕 (Katsuhiko Nishinari)

Dept. of Info. Math., Ryukoku University <sup>1</sup>

One dimensional cellular automaton (CA) models of vehicle traffic and ant traffic are proposed in this paper. These models are closely related to the Burgers CA, which is known as an integrable CA derived by using the ultradiscrete method. Differences between vehicle and ant traffic come from mainly the existence of pheromone in the ant trail model, which allows long range interaction for ants. In the case of vehicle traffic, it is important to consider so-called synchronized state, where both flow and density are high. The model proposed in this paper is shown to reproduce this state around the critical density.

### 1 Introduction

Traffic problems have been attracting not only engineers but also physicists [1]. Especially it has been widely accepted that the phase transition from free to congested traffic flow can be understood using methods from statistical physics [2, 3]. In recent years cellular automata (CA) [4, 5] have been used extensively to study traffic flow in this context. Due to their simplicity, CA models have also been applied by engineers, e.g. for the simulation of complex traffic systems with junctions and traffic signals [6]. Many traffic CA models have been proposed so far [2, 7, 8], and among these CA, the deterministic rule-184 CA model (R184), which is one of the elementary CA classified by Wolfram [4], is the prototype of all traffic CA models. R184 is known to represent the minimum movement of vehicles in one lane and shows a simple phase transition from free to congested state of traffic flow. In a previous paper [9], using the ultra-discrete method [10], the Burgers CA (BCA) has been derived from the Burgers equation

$$v_t = 2vv_x + v_{xx}, \quad (1)$$

---

<sup>1</sup>E-mail: knishi@rins.ryukoku.ac.jp

which was interpreted as a macroscopic traffic model [11]. The BCA is written using the minimum function  $\min$  by

$$U_j^{t+1} = U_j^t + \min\{U_{j-1}^t, L - U_j^t\} - \min\{U_j^t, L - U_{j+1}^t\}, \quad (2)$$

where  $U_j^t$  denotes the number of vehicles at the site  $j$  and time  $t$ . If we put the restriction  $L = 1$ , it can be easily shown that the BCA is equivalent to R184. Thus we have clarified the connection between the Burgers equation and R184, which offers better understanding of the relation between macroscopic and microscopic models. The BCA given above is considered as the *Euler* representation of traffic flow. As in hydrodynamics there is another representation, called *Lagrange* representation [12], which is specifically used for car-following models. The Lagrange version of the BCA is given by [13]

$$x_i^{t+1} = x_i^t + \min\{V_{max}, x_{i+S}^t - x_i^t - S\}, \quad (3)$$

where  $V_{max} = S = L$  and  $x_i^t$  is the position of  $i$ -th car at time  $t$ . Note that in (3)  $S$  corresponds a ‘‘perspective’’ or anticipation parameter [14] which represents the number of cars that a driver sees in front, and  $V_{max}$  is the maximum velocity of cars. (3) is derived from the BCA mathematically by using an Euler-Lagrange (EL) transformation [13] which is a discrete version of the well-known EL transformation in hydrodynamics.

## 2 A new traffic model

In this section we will develop the BCA (3) to a more realistic model by introducing slow-to-start (s2s) effects [15, 16, 17, 18] and a driver’s perspective  $S$ . First, let us extend (3) to the case  $V_{max} \neq S$  and combine it with the s2s model. The s2s model [12] is written in Lagrange form as

$$x_i^{t+1} = x_i^t + \min\{1, x_{i+1}^t - x_i^t - 1, x_{i+1}^{t-1} - x_i^{t-1} - 1\}. \quad (4)$$

Note that the inertia effect of cars is taken into account in this model. Now by combining (3) and (4) we propose a new Lagrange model with general  $S$  as follows:

$$x_i^{t+1} = x_i^t + \min\left\{V_i^t, \min_{k=1, \dots, S-1} (x_{i+k}^t - x_i^t - k + V_{i+k}^t)\right\}, \quad (5)$$

where the last term represents the collision-free condition, and

$$V_i^t = \min\{V_{max}, x_{i+S}^{t-1} - x_i^{t-1} - S, x_{i+S}^t - x_i^t - S, x_i^t - x_i^{t-1} + 1\}. \quad (6)$$

The condition that there is no collision between the  $i$ -th and  $i+k$ -th cars ( $k = 1, \dots, S-1$ ) is given by

$$x_{i+k}^t - x_i^t - k + V_{i+k}^t \geq V_i^t, \quad (7)$$

for  $S \geq 2$  (if  $S = 1$  then we simply put  $k = 1$ ), which is identical to the last term in (5). In contrast to the NS model, the velocity of the preceding car is taken into account in the calculation of the safe velocity, i.e. our model also includes anticipation effects.

### 3 Metastable branches and their stability

Next, we investigate the fundamental diagram of this new hybrid model. In Fig. 1, we

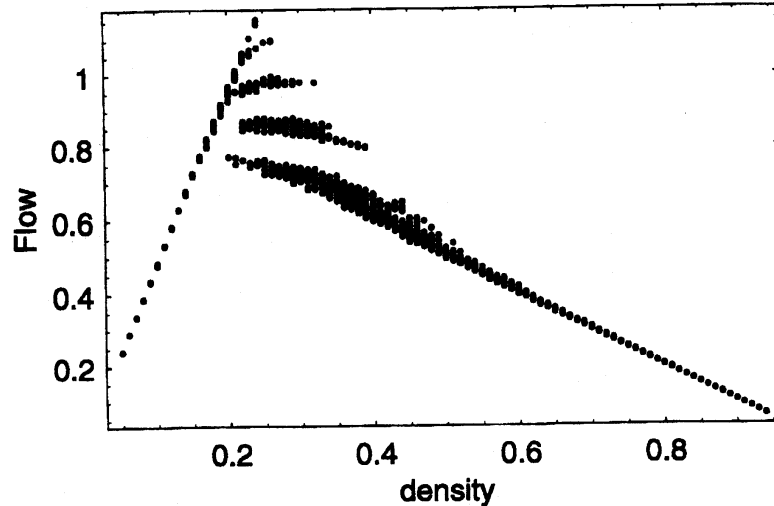


Figure 1: Fundamental diagram of the new Lagrange model. Parameters are set to  $V_{max} = 5$  and  $S = 2$ , and the spatial period is 100 sites. The initial car density is varied from 0.05 to 0.95 in steps of 0.01. At each density, we start calculations from 30 randomly generated initial configurations, and show only the data at the time  $t = 100$ . We observe several metastable branches in the deterministic case. The fluctuations of the branches show the fact that the asymptotic flow of the system sometimes becomes periodic instead of stationary between  $0.2 \leq \rho \leq 0.5$ .

observe a complex phase transition from a free to congested state near the critical density  $0.2 \sim 0.4$ . There are many metastable branches in the diagram, similar to our previous models in Euler form [19, 20] or in other models with anticipation [21]. We also point out that there is a wide scattering area near the critical density in the observed data[22] which may be related to these metastable branches. These branches may account for some aspects of the scattering area observed empirically.

Next let us calculate the flow-density relation for each branch. In the metastable

branches we find phase separation into a free-flow and a jamming region. In the former, pairs move with velocity  $v_f$  and a headway of  $d_f$  empty cells between consecutive pairs. In the jammed region, the velocity of the pairs is  $v_j$  and the headway  $d_j$ .  $N_j$  and  $N_f$  are the numbers of cars in the jamming cluster and the free uniform flow, respectively. We assume  $N_f$  and  $N_j$  to be even so that there are  $N_f/2$  and  $N_j/2$  pairs, respectively. Then the total number of cars  $N$  is given by  $N = N_j + N_f$  and the total length of the system becomes  $l = (d_j + 2)N_j/2 + (d_f + 2)N_f/2$ . Since the average velocity is  $\bar{v} = (N_f v_f + N_j v_j)/N$  and density and flow of the system are given by  $\rho = N/l$  and  $Q = \rho \bar{v}$ , we obtain the flow-density relation as

$$Q = 2 \frac{v_f - v_j}{d_f - d_j} + \left( v_j - (d_j + 2) \frac{v_f - v_j}{d_f - d_j} \right) \rho. \quad (8)$$

It is shown that these branches are generally unstable to perturbations like braking[23].

## 4 The ant-trail model(ATM)

The ants communicate with each other by dropping a chemical (generically called *pheromone*) on the substrate as they crawl forward [24]. Although we cannot smell it, the trail pheromone sticks to the substrate long enough for the other following sniffing ants to pick up its smell and follow the trail. Ant trails may serve different purposes (trunk trails, migratory routes) and may also be used in a different way by different species. Therefore one-way trails are observed as well as trails with counterflow of ants.

In [25] we developed a particle-hopping model, formulated in terms of stochastic CA, which may be interpreted as a model of unidirectional flow in an ant-trail. As in ref. [25], rather than addressing the question of the emergence of the ant-trail, we focus attention here on the traffic of ants on a trail which has already been formed.

Here we define the model which was originally introduced in ref.[25]. Each site of our one-dimensional ant-trail model represents a cell that can accommodate at most one ant at a time (see Fig. 2). The lattice sites are labelled by the index  $i$  ( $i = 1, 2, \dots, L$ );  $L$  being the length of the lattice. We associate two binary variables  $S_i$  and  $\sigma_i$  with each site  $i$  where  $S_i$  takes the value 0 or 1 depending on whether the cell is empty or occupied by an ant. Similarly,  $\sigma_i = 1$  if the cell  $i$  contains pheromone; otherwise,  $\sigma_i = 0$ . Thus, we have two subsets of dynamical variables in this model, namely,  $\{S(t)\} \equiv (S_1(t), S_2(t), \dots, S_i(t), \dots, S_L(t))$  and  $\{\sigma(t)\} \equiv (\sigma_1(t), \sigma_2(t), \dots, \sigma_i(t), \dots, \sigma_L(t))$ . The instantaneous state (i.e., the configuration) of the system at any time is specified completely by the set  $(\{S\}, \{\sigma\})$ .

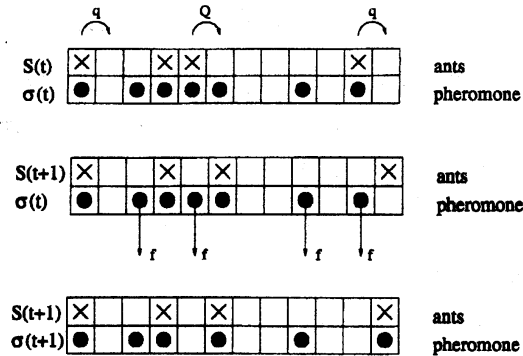


Figure 2: Schematic representation of typical configurations; it also illustrates the update procedure. Top: Configuration at time  $t$ , i.e. *before* stage I of the update. The non-vanishing hopping probabilities of the ants are also shown explicitly. Middle: Configuration *after* one possible realisation of *stage I*. Two ants have moved compared to the top part of the figure. Also indicated are the pheromones that may evaporate in *stage II* of the update scheme. Bottom: Configuration *after* one possible realization of *stage II*. Two pheromones have evaporated and one pheromone has been created due to the motion of an ant.

Since a unidirectional motion is assumed, ants do not move backward. Their forward-hopping probability is higher if it smells pheromone ahead of it. The state of the system is updated at each time step in *two stages*. In stage I ants are allowed to move. Here the subset  $\{S(t+1)\}$  at the time step  $t+1$  is obtained using the full information  $(\{S(t)\}, \{\sigma(t)\})$  at time  $t$ . Stage II corresponds to the evaporation of pheromone. Here only the subset  $\{\sigma(t)\}$  is updated so that at the end of stage II the new configuration  $(\{S(t+1)\}, \{\sigma(t+1)\})$  at time  $t+1$  is obtained. In each stage the dynamical rules are applied *in parallel* to all ants and pheromones, respectively.

### Stage I: Motion of ants

An ant in cell  $i$  that has an empty cell in front of it, i.e.,  $S_i(t) = 1$  and  $S_{i+1}(t) = 0$ , hops forward with

$$\text{probability} = \begin{cases} Q & \text{if } \sigma_{i+1}(t) = 1, \\ q & \text{if } \sigma_{i+1}(t) = 0, \end{cases} \quad (9)$$

where, to be consistent with real ant-trails, we assume  $q < Q$ .

### Stage II: Evaporation of pheromones

At each cell  $i$  occupied by an ant after stage I a pheromone will be created, i.e.,

$$\sigma_i(t+1) = 1 \quad \text{if} \quad S_i(t+1) = 1. \quad (10)$$

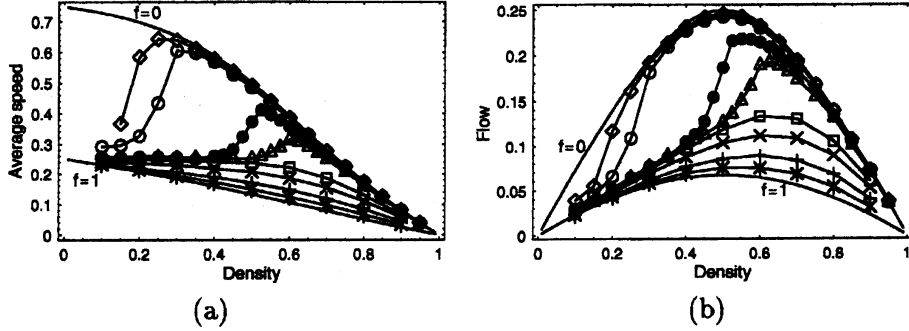


Figure 3: The average speed (a), flux (b) of the ants, extracted from computer simulation data, are plotted against their densities for the parameters  $Q = 0.75, q = 0.25$ . The discrete data points corresponding to  $f = 0.0005(\diamond), 0.001(\circ), 0.005(\bullet), 0.01(\triangle), 0.05(\square), 0.10(\times), 0.25(+), 0.50(*)$  have been obtained from computer simulations; the lines connecting these data points merely serve as the guide to the eye. In (a) and (b), the cases  $f = 0$  and  $f = 1$  are also displayed, which correspond to the NS model with  $q_{\text{eff}} = Q$  and  $q$ , respectively.

On the other hand, any ‘free’ pheromone at a site  $i$  not occupied by an ant will evaporate with the probability  $f$  per unit time, i.e., if  $S_i(t+1) = 0, \sigma_i(t) = 1$ , then

$$\sigma_i(t+1) = \begin{cases} 0 & \text{with probability } f, \\ 1 & \text{with probability } 1 - f. \end{cases} \quad (11)$$

Note that the dynamics conserves the number  $N$  of ants, but not the number of pheromones.

The rules can be written in a compact form as the coupled equations

$$S_j(t+1) = S_j(t) + \min(\eta_{j-1}(t), S_{j-1}(t), 1 - S_j(t)) - \min(\eta_j(t), S_j(t), 1 - S_{j+1}(t)) \quad (12)$$

$$\sigma_j(t+1) = \max(S_j(t+1), \min(\sigma_j(t), \xi_j(t))), \quad (13)$$

where  $\xi$  and  $\eta$  are stochastic variables defined by  $\xi_j(t) = 0$  with the probability  $f$  and  $\xi_j(t) = 1$  with  $1 - f$ , and  $\eta_j(t) = 1$  with the probability  $p = q + (Q - q)\sigma_{j+1}(t)$  and  $\eta_j(t) = 0$  with  $1 - p$ . This representation is useful for the development of approximation schemes.

The flux  $F$  and the average speed  $V$  of vehicles are related by the hydrodynamic relation  $F = \rho V$ . The density-dependence of the average speed in our ATM is shown in Fig. 3(a). Over a range of small values of  $f$ , it exhibits an anomalous behaviour in the sense that, unlike common vehicular traffic,  $V$  is not a monotonically decreasing function of the density  $\rho$ . Instead a relatively sharp crossover can be observed where the speed *increases* with the density. A proper theory of the ATM should reproduce the non-monotonic variation of the average speed with density (shown in Fig. 3(a)) and, hence, the unusual shape of the fundamental diagram (shown in Fig. 3(b)).

## 5 Zero Range Process

It is known that the zero range process(ZRP) is one of the exactly solvable stochastic models. It is a process that the particle hopping probability is related to the number of gaps in front. Thus it is closely related to our ATM, since the hopping probability  $u$  of an ant is given by

$$u(x) = q + (Q - q)g(x) \quad (14)$$

where we take  $g(x) = (1 - f)^{x/v}$ ,  $x$  is the gaps and  $v$  is the mean velocity of ants. Thus by using the ZRP, the average velocity  $v$  of ants is calculated by

$$v = \sum_{x=1}^{L-M} u(x)p(x) \quad (15)$$

where  $L$  and  $M$  are the system size and the number of ants respectively (hence  $M/L$  is the density), and

$$p(x) = h(x) \frac{Z(L-x-1, M-1)}{Z(L, M)}, \quad (16)$$

where  $Z$  is the partition function and  $h(x)$  can be calculated as[27]

$$h(x) = \begin{cases} 1 - u(1) & \text{for } x = 0 \\ \frac{1 - u(1)}{1 - u(x)} \prod_{y=1}^x \frac{1 - u(y)}{u(y)} & \text{for } x > 0 \end{cases} \quad (17)$$

The partition function  $Z$  is obtained by the recurrence relation

$$Z(L, M) = \sum_{x=0}^{L-M} Z(L-x-1, M-1)h(x), \quad (18)$$

with  $Z(x, 1) = h(x-1)$  and  $Z(x, x) = h(0)$ .

By using these formulae, we obtain the following fundamental diagram. We could set at most  $L = 200$  up to now because of the numerical precision restriction. Fundamental diagram of ATM is given by the figure 4. The black curve with circles is the numerical data, and the simple black curve is the theoretical curve calculated by using ZRP. System size is  $L = 100$ (Fig.4(a)) and  $L = 200$ (Fig.4(b)). Parameters are  $Q = 0.75$ ,  $q = 0.25$ ,  $f = 0.001$ . We see that the theoretical curve approaches to the numerical one if we take larger  $L$ 's.

## 6 Concluding discussions

In this paper we have proposed a new hybrid model of traffic flow of Lagrange type which is a combination of the BCA and the s2s model. The model shows several metastable

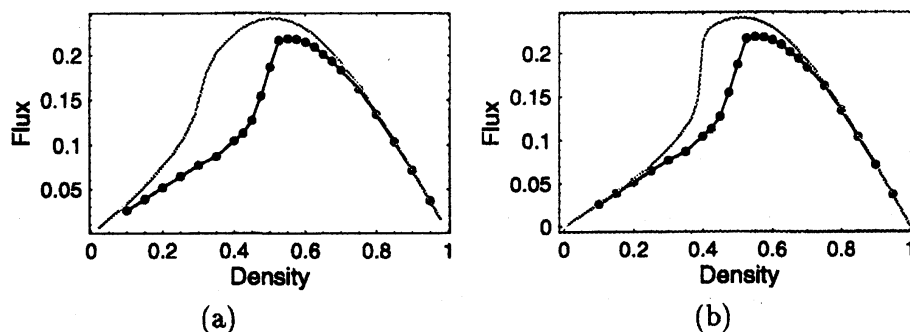


Figure 4: Comparison of the results by using ZRP with simulations in the case of (a)  $Z = 100$  and (b)  $Z = 200$ .

branches around the critical density in its fundamental diagram. The upper branches are unstable and will decrease its flow under perturbations. Moreover, we have shown a new ant traffic model by taking into account the effect of pheromone. The fundamental diagram shows unusual velocity-density relation, which is analyzed by using the zero range process.

## References

- [1] D. Helbing and H. J. Herrmann and M. Schreckenberg and D. E. Wolf (eds.), "Traffic and Granular Flow '99", (Springer, 2000, Berlin).
- [2] D. Chowdhury, L. Santen and A. Schadschneider, Phys. Rep. **329** (2000) 199.
- [3] D. Helbing, Rev. Mod. Phys., **73** (2001) 1067.
- [4] S. Wolfram, *Theory and applications of cellular automata*, (World Scientific, 1986, Singapore).
- [5] B. Chopard and M. Droz, *Cellular Automata Modeling of Physical Systems*, (Cambridge University Press, 1998).
- [6] S. Bandini, R. Serra and F. S. Liverani (eds.), *Cellular Automata: Research Towards Industry*, (Springer, 1998).
- [7] M. Fukui and Y. Ishibashi, J. Phys. Soc. Jpn. **65** (1996) 1868.
- [8] K. Nagel and M. Schreckenberg, J. Phys. I France **2** (1992) 2221.
- [9] K. Nishinari and D. Takahashi, J. Phys. A. **31** (1998) 5439.

- [10] T. Tokihiro, D. Takahashi, J. Matsukidaira, and J. Satsuma, Phys. Rev. Lett. **76** (1996) 3247.
- [11] T. Musya and H. Higuchi, J. Phys. Soc. Jpn. **17** (1978) 811.
- [12] K. Nishinari, J. Phys. A **34** (2001) 10727.
- [13] J. Matsukidaira and K. Nishinari, Phys. Rev. Lett. **90** (2003) 088701.
- [14] K. Nishinari and D. Takahashi, J. Phys. A **33** (2000) 7709.
- [15] M. Takayasu and H. Takayasu, Fractals **1** (1993) 860.
- [16] S.C. Benjamin and N.F. Johnson, J. Phys. A **29** (1996) 3119.
- [17] A. Schadschneider and M. Schreckenberg, Ann. Physik **6** (1997) 541.
- [18] R. Barlovic, L. Santen, A. Schadschneider, and M. Schreckenberg, Eur. Phys. J. **5** (1998) 793.
- [19] K. Nishinari and D. Takahashi, J. Phys. A., **32** (1999) 93.
- [20] M. Fukui, K. Nishinari and D. Takahashi and Y. Ishibashi, Physica A, **303** (2002) 226.
- [21] M.E. Larraga, J.A. del Rio and A. Schadschneider, (2003) cond-mat/0306531.
- [22] K. Nishinari and M. Hayashi, *Traffic statistics in Tomei express way*, (The Mathematical Society of Traffic Flow, 1999, Nagoya).
- [23] K. Nishinari, M. Fukui and A. Schadschneider, to be published in J.Phys.A.
- [24] E.O. Wilson, *The insect societies* (Belknap, Cambridge, USA, 1971); B. Hölldobler and E.O. Wilson, *The ants* (Belknap, Cambridge, USA, 1990).
- [25] D. Chowdhury, V. Guttal, K. Nishinari and A. Schadschneider, J. Phys. A:Math. Gen. **35**, L573 (2002).
- [26] Nishinari, K., D. Chowdhury and A. Schadschneider, Phys. Rev. E **67**, p.036120 (2003).
- [27] M. R. Evans, J. Phys. A:Math. Gen. **30**, p.5669 (1997).